Nano Energy 26 (2016) 43–49

Contents lists available at ScienceDirect

Nano Energy

journal homepage: www.elsevier.com/locate/nanoen

In-situ activated polycation as a multifunctional additive for Li-S batteries

Hongwei Chen [a,1], Changhong Wang [a,1], Yafei Dai [b], Jun Ge [a], Wei Lu [a], Jinlong Yang [c], Liwei Chen [a,d,*]

[a] *i-Lab, CAS Center for Excellence in Nanoscience, Suzhou Institute of Nano-Tech and Nano-Bionics, Chinese Academy of Sciences, Suzhou 215123, China*
[b] *Jiangsu Key Laboratory of Optoelectronic Technology, School of Physics Science & Technology, Nanjing Normal University, Nanjing 210023, China*
[c] *Hefei National Laboratory for Physical Sciences at Microscale, University of Science and Technology of China, Hefei, Anhui 230026, China*
[d] *Vacuum Interconnected Nanotech Workstation, Suzhou Institute of Nano-Tech and Nano-Bionics, Chinese Academy of Sciences, Suzhou 215123, China*

ARTICLE INFO

Article history:
Received 18 February 2016
Received in revised form
24 April 2016
Accepted 30 April 2016
Available online 2 May 2016

Keywords:
Electrochemistry
Energy storage
Lithium-sulfur batteries
Radical polymer
Functional additive

ABSTRACT

While Li–S batteries are poised to be the next generation high-density energy storage devices, the low sulfur utilization and intrinsic polysulfide shuttle have limited their practical applications. Here, we report that radical polymer Poly(2,2,6,6-tetramethyl-1-piperidinyloxy-4-yl methacrylate) (PTMA)—a stable free radical polymer reported to be potential organic electrode materials–can perform as a multifunctional sulfur-trapping and catalytic binder for high performance Li-S batteries once activated via *in-situ* electrochemical oxidation. The activated $PTMA^+$ not only displays strong binding affinity to polysulfides but also provides $PTMA^+$-assisted additional redox sites and improves the kinetics of the cathode reaction. Thus the novel multifunctional additive for Li-S batteries results in improved cycle life, faster rate performance and most importantly, a significantly increase in specific discharge capacity by ~80%, with specific capacity of 1254 mAh/g and Coulombic efficiency of 96% at a four-hour charge/discharge (C/4) current rate.

1. Introduction

The lithium-sulfur (Li-S) battery, with theoretical specific energy of 2600 Wh/kg, has been considered a promising candidate as the next generation energy storage technology beyond Li ion batteries (LIB) [1]. The operating mechanism of Li-S battery is based on a series of redox reactions between elemental sulfur (S_8) and its lithiated derivatives $Li_2S_n^{2-}$ ($1 \leq n \leq 8$) with a complex solid-liquid-solid phase transition in the cathode, and a reversible lithium metal stripping/plating process at the anode [2]. After almost three decades of development, implementing the Li-S battery technology for commercial systems still remains a challenge [3,4]. The major obstacles are short cycling life and less-than-theoretical use of sulfur. These problems are related to the dissolution of lithium polysulfide intermediates in liquid electrolyte and the consequent parasitic reactions in addition to other reasons such as poor current collection and electrode structures [5]. Much of previous work to improve cycling life builds on ideas of designing porous carbon-based cathode materials that are capable of trapping soluble polysulfides by physical confinement [6–8]. Recently, tailor-designed polysulfide trapping materials have emerged to improve the interaction between the cathode material with polar polysulfide species [9,10]. In particular, surface-functionalized carbon materials and metal oxides with polar metal–O bonds have shown their effectiveness in improving cycle stability through chemisorption [11–14].

In a typical Li-S cathode, the majority of the discharging capacity comes from the reduction of dissolved polysulfide intermediates [15]. The ideal Li-S cathode structure, therefore, shall on one hand contain effective polysulfide trapping sites to limit polysulfide shuttling and thus improve the cycle life, and on the other hand shall also render these trapped polysulfide electrochemically active to ensure high specific capacity. The success of such a strategy has been manifested in recent reports that nitrogen-doped carbon composites, conductive titanium carbide Ti_2C nanosheets and ternary hybrid materials as special host materials in Li-S cathode result in enhanced capacity and improved cycle stability [16–18].

Here we report a new multifunctional polymer additive for Li-S batteries–poly(2,2,6,6-tetramethylpiperidinyloxy-4-yl methacrylate) (PTMA)—that not only replaces conventional binders such as PVDF to stabilize the cathode structure, but also traps polysulfide

* Corresponding author at: *i*-Lab, CAS Center for Excellence in Nanoscience, Suzhou Institute of Nano-Tech and Nano-Bionics, Chinese Academy of Sciences, Suzhou 215123, China.
E-mail address: lwchen2008@sinano.ac.cn (L. Chen).
[1] These authors contributed equally to this work.

http://dx.doi.org/10.1016/j.nanoen.2016.04.052
2211-2855/

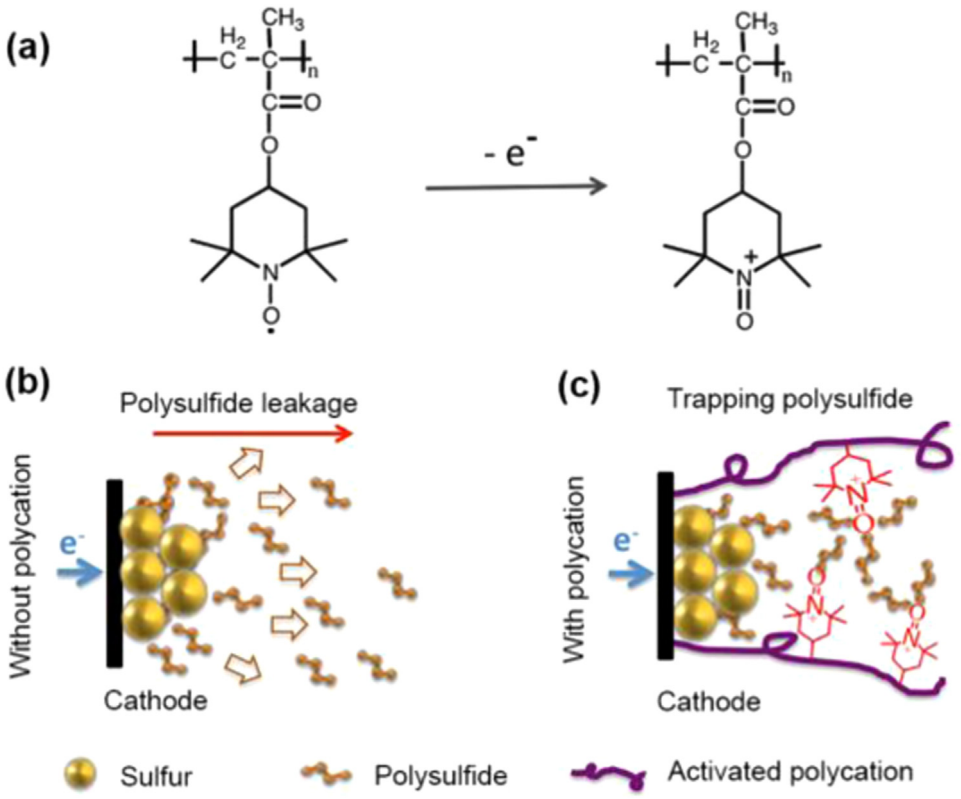

Fig. 1. Schematic illustration of the PTMA multi-functional binder. (a) *In-situ* activation of PTMA to polycation by charging to 4.0 V. (b) Conventional Li-S cathodes without the PTMA binder. (c) Li-S cathode with activated PTMA polycation. Polysulfide interacting with the electrochemically activated trapping sites is electrochemically accessible to the conducting carbon electrode.

intermediates once activated via *in-situ* electrochemical oxidation at the Li-S cathode (Fig. 1). The activated PTMA exists in the form of polycations and is also observed to accelerate the cathode kinetics. Overall, the PTMA binder results in improved cycle life, faster rate performance and most importantly, a significantly increase in specific capacity by ~80%.

2. Experimental section

2.1. Chemicals and materials

Sulfur powder (99.9%) was purchased from Aldrich. rGO was purchased from Nanjing JC nano Tech Co., Ltd. Ethylene diamine anhydrous (EDA, analytical grade), anhydrous ethanol, anhydrous methanol, ethyl ether, N-methyl pyrrolidone (NMP), acetone and 30% H_2O_2 were purchased from Sinopharm Chemical Reagent Co., Ltd. 2,2,6,6-tetramethylpiperidine methacrylate (MTMP), ethylenediaminetetraacetic acid (EDTA) were purchased from TCI. 2,2′-azobisisobutyronitrile (AIBN), $Na_2WO_4 \cdot 2H_2O$ were purchased from Sigma Chemical Co.

2.2. Synthesis of PTMA

MTMP monomer (4.5 g, 20 mmol) and AIBN (0.07 g, 0.42 mmol) were added into 15 mL of acetic acid. The mixture was stirred at 70 °C for 12 h under N_2 atmosphere. Then the reaction mixture was added to 100 mL of ethyl ether and stirred. The product PMTMP was obtained by filtration. The as-synthesized PMTMP (1.5 g, 12.4 mmol) in 30 mL methanol, $Na_2WO_4 \cdot 2H_2O$ (0.45 g, 1.35 mmol), ethylenediaminetetraacetic acid (EDTA) (0.3 g, 1.02 mmol), 30% H_2O_2 (4 mL) and H_2O (15 mL) were added to a beaker and stirred at 60 °C for 48 h. The mixture was filtered and washed with H_2O and ethyl ether. After dried at 50 °C in vacuum, the obtained PTMA is a pale red solid.

2.3. Preparation of PTMA containing sulfur cathodes

A 1:4 weight ratio rGO/sulfur composite was prepared via ball milling. The rGO/sulfur composite was then mixed with carbon black and the synthesized PTMA with a weight ratio of 7:2:1 in NMP with vigorous stirring for 24 h to form a cathode slurry. The slurry was coated onto an aluminum collector and baked at 60 °C for 24 h to form a cathode. The control experiment with the PVDF binder used the exact same procedure except that the PTMA was replaced by the same amount of PVDF. The mass loading of the sulfur in the cathode is ~1.8–2.0 mg/cm^2.

The pure PTMA electrode was prepared via a dispersing-depositing process: 10% PTMA was first dissolved in NMP, 20% carbon black was added into the solution and stirred 30 min. Then 60% graphene and 10% PVDF NMP solution was added into the above solution under stirring for 24 h to form a cathode slurry. The slurry was coated onto an aluminum collector and baked at 60 °C to form a cathode.

2.4. Cell assembly and electrochemical testing

Coin-type (CR2025) cells were fabricated by sandwiching a porous polypropylene separator between a cathode containing the active materials and a lithium metal foil in a high-purity argon-filled glove box. The electrolyte used was 1 M LiTFSI in a solvent mixture of DOL/DME (1:1 v/v) without $LiNO_3$ unless specifically noted otherwise. The lithium foil anode for the coin cell testing was used without any pretreatment. The diameter of the cathode is 1.5 cm. A total of 70 μl electrolyte was used in each battery. The cells were discharged and charged on a battery test system

(NEWARE, NEWARE technology Ltd. Shenzhen) from 1.5 to 2.8 V at a current density of 400 mA/g unless specifically noted. LSV (linear sweep voltammetry) measurements were conducted in a three-electrode system with a lithium polysulfide solution serving as the electrolyte. The scan rate of 50 mV s^{-1} at a rotation rate of 1000 rpm was used for the measurements. A glassy carbon rotating disk electrode (RDE, Pine Instruments Co.) was used as the working electrode. The polymer solution (0.05 wt% in NMP, 20 µl) was loaded onto the surface of glassy carbon disk followed by drying. Metallic lithium strips were used as both counter and reference electrode. The lithium strips were firstly covered with a passivation layer on the surface by soaking the lithium strip in 1 M LiTFSI in DOL/DME solution with 1 wt% $LiNO_3$ additive for 2 h. To prepare lithium polysulfide solution, stoichiometric amounts of Li_2S and sulfur were mixed together with a nominal formula of Li_2S_8 and stirred in DOL/DME (1:1 v/v) at 50 °C overnight. 0.2 M solution was prepared for the LSV.

2.5. Characterizations

The as-prepared samples were characterized using a Scanning Electron Microscope (SEM) (FEI Quanta 400 FEG) equipped with Energy Dispersive X-ray Microanalysis (EDX) (Apollo 40 SDD). EPR (electron paramagnetic resonance) measurements were performed in a continuous wave X-band spectrometer (JEOL, JES-FA200) at room temperature. The samples are measured at a microwave power of 0.998 mW and a microwave frequency of 9066 ± 3 MHz. X-ray photoelectron spectroscopy study was performed on a SSI S-Probe XPS spectrometer. The samples were transferred into the analysis chamber of the XPS spectrometer by a transfer device, which prevented contact with air. Fourier transform infrared (FTIR) spectra were collected using a Thermo Scientific Nicolet 6700 spectrometer by dispersing samples in KBr pellets. Cyclic voltammetry (CV) scans were performed on a CHI 660 C electrochemical workstation (CHI Instruments, Inc.) at a scan rate of 0.1 mV s^{-1}.

3. Results and discussion

PTMA was synthesized according to a previously published procedure and the Fourier transform infrared spectroscopy of the product is shown in Fig. S1 [19]. In order to highlight the role of the multifunctional binder, coin cells with a simple cathode structure containing ball-milled elemental sulfur, reduced-graphene oxide (rGO), carbon black, and the binder were prepared to test the electrochemical performance. Since the side chain of PTMA may undergo a reversible redox transformation between the nitroxide radical NO● form and the oxidized oxoammonium cation NO^+ form with an standard equilibrium potential at ~3.6 V, two different cycling modes were applied for the PTMA-containing cathodes [19]. One mode is *in-situ* activating PTMA to NO^+ cations ($PTMA^+$) by charging to 4.0 V first, and then cycling in the Li-S window of 1.5–2.8 V in subsequent cycles (named as $PTMA^+$/S battery). A control experiment is simply cycling the battery at the 1.5–2.8 V window without activation to NO^+ cations (named as PTMA/S battery). Another control experiment is the cathode prepared using the same materials and the same ball milling method except using the traditional PVDF binder. This battery was charged to 4.0 V for "activation" before regular cycling (named as PVDF/S battery). 1 M LiTFSI in 1,3-dioxolane and 1,2-dimethoxyethane (DOL/DME 1:1) electrolyte was used in all cells unless otherwise specified. Scanning electron microscopy (SEM) images (Fig. S2) of as-prepared cathodes showed typical morphology of mixed pastes with well-dispersed carbon and sulfur elements.

Fig. 2 presents the electrochemical performances of the three cells. The PTMA/S and $PTMA^+$/S batteries showed drastically different performances: $PTMA^+$/S exhibited remarkable enhancements in both capacity and cycling stability. The initial galvanostatic discharge capacity of PTMA/S is 692 mAh/g (the red curve in Fig. 2(a)), while that of the $PTMA^+$/S is 1254 mAh/g (the blue curve in Fig. 2(a)), increased by nearly 80%. Note that the $PTMA^+$/S battery displayed a charging plateau of 120 mAh/g at ~3.6 V during the activation stage (inset of Fig. 2(a)), which indicated that

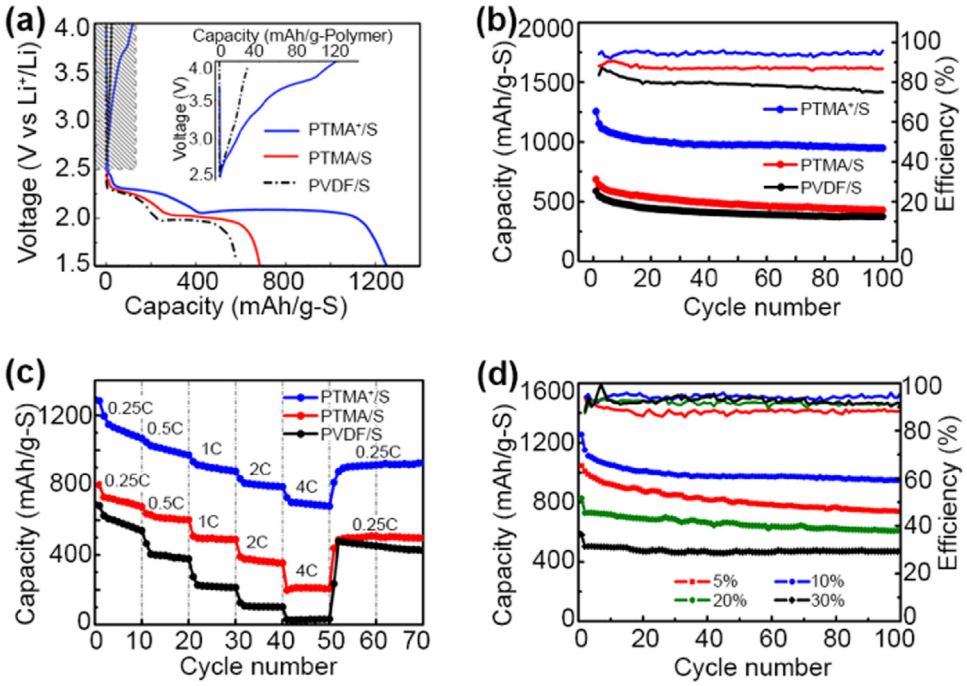

Fig. 2. Electrochemical performances of Li-S batteries. (a) Initial galvanostatic discharge/charge curves of different batteries, PTMA/S (1.5–2.8 V), $PTMA^+$/S (1.5–4.0 V), PVDF/S (1.5–4.0 V). (b) Cycling performance of PTMA/S, $PTMA^+$/S, and PVDF/S batteries at a current density of 400 mA/g. (c) Rate performances of $PTMA^+$/S, PTMA/S, and PVDF/S batteries. (d) Cycling performance of $PTMA^+$/S batteries with different PTMA contents at a current density of 400 mA/g. (For interpretation of the references to color in this figure, the reader is referred to the web version of this article).

the NO● have been oxidized to NO^+ [19]. The cyclic voltammetry curve also confirmed the oxidization process (Fig. S3). Considering the full charge capacity of ~175 mAh/g in pure PTMA battery (Fig. S4a), ~68% of NO● groups was oxidized in PTMA$^+$/S cathode, and the remaining NO● is about 32%. An interesting fact is that the subsequent discharge curve shows no discharging plateau at 3.6 V, suggesting that NO^+ groups are not reduced back to NO● in subsequent cycling in the PTMA$^+$/S battery. Both PTMA/S and PTMA$^+$/S batteries show higher capacities than the control PVDF/S battery (608 mAh/g, the black curve in Fig. 2(a)). The PTMA$^+$/S battery possesses the highest Coulombic efficiency of ~96% and capacity retain ratio of ~75% after 100 cycles, while these decreased to ~88% and 62% for PTMA/S battery, ~80% and 66% for PVDF/S battery, respectively (Fig. 2(b)). Even after 500 cycles, the PTMA$^+$/S battery shows a capacity of ~625 mAh/g, which is significantly higher than the control cells (Fig. S5). The PTMA$^+$/S battery also shows improved rate performances compared to the control batteries (Fig. 2(c)). It exhibits a reversible capacity of ~690 mAh/g at 6400 mA/g (4 °C) after more than 40 cycles at various rates, and then exhibits a reversible capacity of ~900 mAh/g with further cycling back at 400 mA/g (0.25 °C). It is also found that the PTMA$^+$/S battery reaches the best performances at 10 wt% PTMA content; higher PTMA content leads to significant decline in performances, which may be ascribed to that the electron/ion transfer paths inside cathode would be partially blocked as un-activated binder increased (Fig. 2(d)).

To our knowledge, such *in-situ* activated performance improvement is rarely reported in Li-S batteries. According to the discharge/charge curves in Fig. 2(a), after activated to 4.0 V, the *in-situ* generated NO^+ is likely to persist in the cathode in the subsequent cycles, which hints that NO^+ cations play an important role in discharging/charging processes. Electron paramagnetic resonance (EPR) further verified the irreversible oxidation process in the PTMA$^+$/S battery. As shown in Fig. 3, original PTMA$^+$/S (before activation) produced a broad EPR signal due to the high density of the unpaired electrons from the NO● radical in PTMA molecules [20]. The signal is significantly weakened when charged to 4.0 V, suggesting the loss of unpaired electrons as a majority of the NO● radicals were oxidized to NO^+. The EPR signal remained almost unchanged in the following discharging cycles to as low as 2.0 V (comparing to the ~3.6 V redox potential of NO^+). It confirms that the majority of NO^+ is not reduced back to NO● and further underlines the important role of NO^+ in cycling.

Hence, *ab initio* calculations in the framework of density functional theory (DFT) were carried out to gain an understanding of the NO^+-polysulfide interaction. The electronic structure of PTMA/PTMA$^+$ molecules was calculated firstly. The repeating unit of PTMA with a NO● group on the side chain possesses a single electron in its highest occupied molecular orbital (HOMO), and this orbital

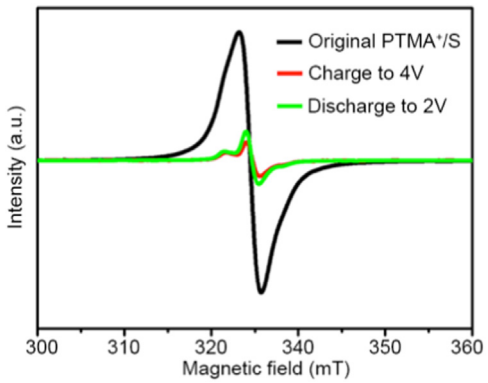

Fig. 3. EPR of PTMA$^+$/S battery at different voltage stages.

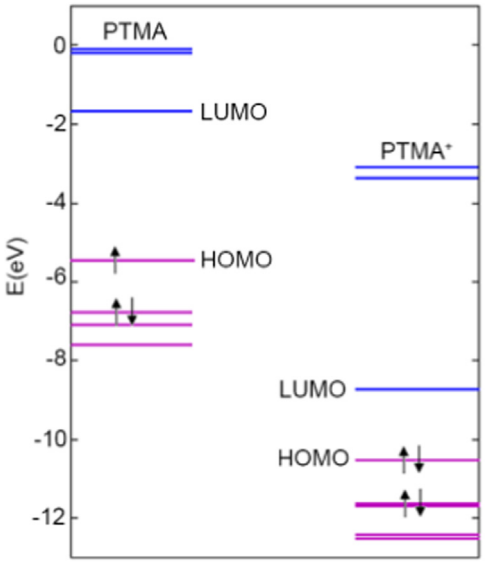

Fig. 4. Calculated molecular orbital energies for relaxed PTMA and PTMA$^+$ molecules.

becomes empty when NO● is oxidized into NO^+ (Fig. 4). A series of S_n^{2-} (n=2, 4, 6, and 8) were used to represent the general class of polysulfides in calculating their binding energy with the NO^+ group. In all cases, the [NO^+-S_n^{2-}] interaction exhibits much higher binding energy than the corresponding [NO●-S_n^{2-}] interaction (see data and details in Table S1). This indicates that the polysulfide trapping property is activated when NO● is oxidized into NO^+. Apparently, the strong electrostatic attraction between NO^+ cations and S_n^{2-} anions is a major contribution to the ultrahigh binding energies. Interestingly, an additional coordination-like interaction may also exist between polysulfides and the PTMA$^+$ polycations. Mulliken charge distribution of S_8^{2-} reveals that the −2 net charge on the S atom in S_8^{2-} is reduced to −0.69 when S_8^{2-} interacts with NO^+. A similar trend is observed in other polysulfide species. This agrees with the intuition that the lone pair electrons in S atoms of polysulfides may interact with the empty molecular orbital of NO^+ through a coordination-like interaction [21].

The strongly interacting intermediates between NO^+ and S_n^{2-} are experimentally confirmed with X-ray photoelectron spectroscopy (XPS). The PTMA$^+$/S and the pure PTMA cathodes were both activated to 4 V first and then discharged to 2.0 V in DOL/DME electrolyte before XPS measurements. It should be noted that in contrast to the rechargeable pure PTMA cathode in ester electrolyte (EC/DMC), the pure PTMA cathode in ether electrolyte (DOL/DME) can be charged to NO^+ but cannot be discharged back to NO● (Fig. S4). This is reasonable considering that the NO^+ may also be capable of binding with the ether groups, where the lone electron pairs on oxygen atoms may interact with NO^+ through similar coordination-like interactions. The two N_{1s} peaks of the pure PTMA cathode at ~399.54 and ~401.69 eV (Fig. 5(a)) are attributed to the unreacted NO● and the NO^+-ether complex, respectively [22]. In the PTMA$^+$/S cathode, similar peaks of NO● and NO^+-ether complex are observed at ~398.99 and ~401.69 eV, respectively; and importantly, a new N_{1s} peak emerged at 400.76 eV (Fig. 5(b), see detail in Table S2). The location of the new peak is at a lower binding energy than that of the NO^+-ether complex, and is thus speculated to result from the [NO^+-S]$^+$ complex because S has stronger electron-donating capability than O atom, which shall lead to a lower formal oxidation state in N atom and a smaller N_{1s} binding energy [22]. As not all NO● groups on the polymer can diffuse to the conducting network in the electrode structure and become electrochemically active, there

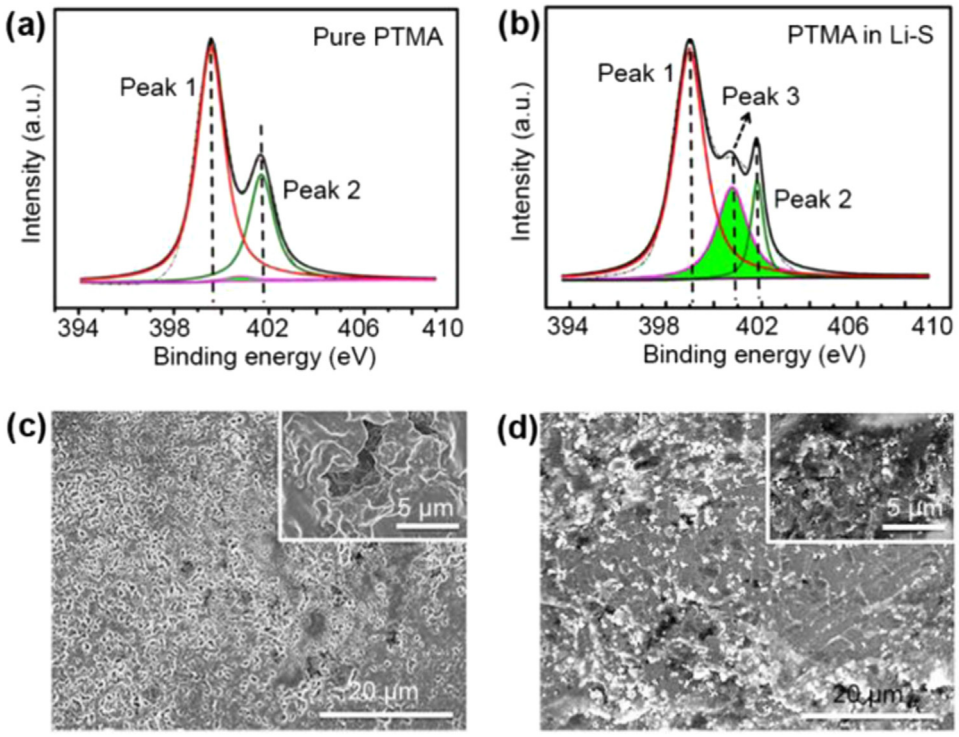

Fig. 5. XPS spectra of (a) pure PTMA cathode discharged to 2.0 V, and (b) $PTMA^+$/S cathode discharged to 2.0 V. Both cathode were activated first and then cycled in DOL/DME electrolyte. SEM micrographs of the Li anode surface after 100 cycles in (c) PTMA/S battery, and (d) $PTMA^+$/S battery.

would be a little more NO● groups remain on electrode surface. Taking into consideration that the information depth of XPS is in a range of several nanometers, it is reasonable that the more residual NO● groups were detected based on XPS tool.

This interaction between $PTMA^+$ and polysulfide has significant impacts on the electrochemical performance of the $PTMA^+$/S battery. First of all, the polysulfide binding property improves the cycle stability. The diffusion of polysulfide is limited when they are "trapped" on *in-situ* activated $PTMA^+$ polycations, and thus the polysulfide shuttle effect is suppressed. The polysulfide trapping effect is supported by the Li anode morphology data. After 100 cycles, the Li surface of PTMA/S battery becomes porous (Fig. 5(c)) since the Li anode is aggressively corroded by polysulfides as the shuttle effect takes place. Lithium sulfides and side products of Li anode reacting with electrolyte are randomly deposited on the anodic surface as a result of inhomogeneous local current densities [23,24]. On the other hand, Li anodic surface in the $PTMA^+$/S battery is much smoother (Fig. 5(d)), indicating significantly alleviated polysulfide shuttling. It also can be confirmed by the less degradation of $PTMA^+$/S cathode configuration (Fig. S6). Similar improvements in cycle stability have been reported previously in other chemisorption (such as Lewis acid-base interactions)-based polysulfide-trapping systems [9,25–28]. However, unique to this *in-situ* activated sulfur-trapping agent is that the specific capacity and the rate performance are also enhanced simultaneously.

The drastically improved specific capacity and rate performance of $PTMA^+$/S battery (Fig. 2(a) and (c)) arise from the unique cathode structure containing *in-situ* activated $PTMA^+$. Firstly, the activated $PTMA^+$ cations are capable of assisting polysulfide reduction. Although the polymer backbone of PTMA is electrically insulating and insoluble in electrolyte, those NO● side-chain groups adjacent to the conducting carbon network may still diffuse to the conducting network via the motion of polymer chain segments, lose an electron, and become oxidized into NO^+ during the activation process. The polysulfide anions trapped to the $PTMA^+$ groups then may also get access to the conducting carbon network via chain segment motion in subsequent cycles. Therefore, the activated $PTMA^+$ groups adjacent to the conducting network become extra reaction sites where the $PTMA^+$ groups assist the redox reaction, in addition to the usual reaction sites where sulfur particles and polysulfide anions are directly in contact with the conducting network (Fig. 6). The extra reactive sites allow those active materials in the cathode (including S_8 and polysulfide intermediates) that would otherwise have no access to the conducting network to undergo the cathode reaction, and thus significantly improve the sulfur utilization and the specific capacity.

Secondly, DFT calculations and linear sweep voltammetry (LSV) show that $PTMA^+$ exhibits catalytic activity towards the cathode reaction. The DFT calculated results (Table 1) indicate that all $[NO^+\text{-}S_n^{2-}]$ species exhibit higher electron affinity (EA) than $[S_n^{2-}]$ (see detail in SI, here $EA = E_{molecule}^- - E_{molecule}$, thus smaller numerical value means higher EA) (Table S1). Since the higher EA suggests the lower lowest unoccupied molecular orbital (LUMO) level and the higher reduction potential, $[NO^+\text{-}S_n^{2-}]$ is more readily reduced than $[S_n^{2-}]$ [29,30]. This effect was confirmed by LSV measurements (see detailed measurement in SI). Higher

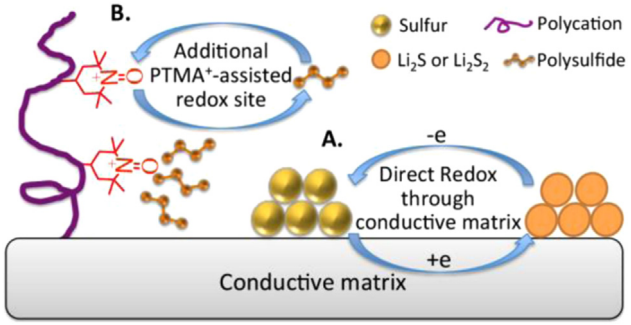

Fig. 6. Schematic illustration of the redox processes inside the cathode with activated $PTMA^+$. (A) Redox through the conductive matrix; (B) $[NO^+\text{-}S_n^{2-}]$ intermediate-assisted polysulfide redox.

Table 1
Initial discharging capacity at different stages.

	$PTMA^+$/S	PTMA/S	PVDF/S
S-to-L stage (mAh/g)	~235	~182	~150
L-to-S stage (mAh/g)	~1019	~510	~458
L-to-S/S-to-L[a]	4.34	2.80	3.05

[a] Complete utilization of sulfur in the solution phase corresponds to L-to-S/S-to-L=5. See detailed discussion in SI.

limiting current was obtained in the $PTMA^+$ electrode, as compared with the conventional PVDF electrodes (Fig. S7), suggesting more efficient reduction of the polysulfide in [NO^+-S_n^{2-}]. The reduced polarization of the low-voltage plateau in $PTMA^+$/S battery (Fig. 2(a)) is another evidence supporting the improvement of polysulfide reduction kinetics. The enhanced reaction kinetics thus contributes to improved rate performance of the cell.

Therefore, the improved discharging capacity and rate performance of $PTMA^+$/S batteries originate from: (1) the strong interaction between NO^+ and S_n^{2-}; and (2) $PTMA^+$-assisted additional reaction sites and enhanced reactivity towards the polysulfide reduction of [NO^+-S_n^{2-}] species. Since these mechanisms are mostly effective towards the dissolved polysulfide species, it can be expected that the portion of discharge capacity corresponding to polysulfide reduction in the solution phase (the L-to-S stage, see discussion in SI) shall increase with respect to the capacity corresponding to the solid-solution transformation from S_8 to S_8^{2-} (the S-to-L stage). Detailed analyses of the initial discharge curves in Fig. 2(a) indeed confirm this hypothesis. As shown in Fig. S9, the specific capacity corresponding to the S-to-L stage and to the L-to-S stage in the $PTMA^+$/S, PTMA/S, and PVDF/S batteries are analyzed and the results are summarized in the Table 1. The ratio between the capacities of the two portions is a good indication of how efficient the solution phase reduction is during discharge. While the theoretical value of this ratio shall be 5, the ratio in the $PTMA^+$/S battery reached 4.3, indicating efficient reduction of polysulfides due to the presence of the $PTMA^+$ multifunctional binder. In comparison, the ratio in PTMA/S and PVDF/S batteries are 2.8 and 3.0 respectively, indicating inefficient utilization of polysulfides in solution [31–34]. The efficiency of polysulfide reduction in $PTMA^+$/S batteries gradually decreased during cycling (Fig. S10).

4. Conclusion

In summary, PTMA has been demonstrated as a multi-functional additive in Li-S cathode, which not only replaces conventional binders such as PVDF, but also significantly improves battery performance once PTMA is *in-situ* activated. The most important feature of the activated $PTMA^+$ is the strong binding affinity with polysulfides, moreover, it is also demonstrated to provide $PTMA^+$-assisted additional redox sites and improve the kinetics for the cathode reaction. Consequently, the PTMA not only improves the cycle stability via suppression of polysulfide shuttling, which is commonly observed with other sulfide-trapping agents, but also uniquely improves the specific capacity and rate performance. It is important to realize the dominating contribution of solution-phase redox steps in Li-S capacity. Thus by focusing on improving the utilization of polysulfides in the solution-phase, the PTMA helps to achieve an initial specific capacity of 1254 mAh/g at a sulfur loading of 80%. It is worth noting that the excellent cycle stability, specific capacity, and rate performance are achieved in a simply ball-milled cathode mixture. Such cathode structures are highly convenient and economical for large-scale practical applications, but have previously stuck with inferior battery performance. With the demonstration of the PTMA multi-functional additive, further advances towards high-performance Li-S battery can be expected considering the almost unlimited possibility in molecular design and synthesis.

Acknowledgments

The authors acknowledge funding support from the Strategic Priority Research Program of the CAS, Grant no. XDA09010600, the National Natural Science Foundation of China (21473242, 21273273) and the Collaborative Innovation Center of Suzhou Nano Science and Technology. L.C. acknowledges Natural Science Foundation of Jiangsu Province for support (BK20130006).

Appendix A. Supplementary material

Supplementary data associated with this article can be found in the online version at http://dx.doi.org/10.1016/j.nanoen.2016.04.052.

References

[1] P.G. Bruce, S.A. Freunberger, L.J. Hardwick, J.-M. Tarascon, Nat. Mater. 11 (2012) 19–29.
[2] Z. Deng, Z. Zhang, Y. Lai, J. Liu, J. Li, Y. Liu, J. Electrochem. Soc. 160 (2013) A553–A558.
[3] E. Peled, A. Gorenshtein, M. Segal, Y. Sternberg, J. Power Sources 26 (1989) 269–271.
[4] A. Rosenman, E. Markevich, G. Salitra, D. Aurbach, A. Garsuch, F.F. Chesneau, Adv. Energy Mater. (2015), http://dx.doi.org/10.1002/aenm.201500212.
[5] S.S. Zhang, J. Power Sources 231 (2013) 153–162.
[6] Y. Yang, G. Zheng, Y. Cui, Chem. Soc. Rev. 42 (2013) 3018–3032.
[7] M.A. Pope, I.A. Aksay, Adv. Energy Mater. (2015), http://dx.doi.org/10.1002/aenm.201500124.
[8] Y.X. Yin, S. Xin, Y.G. Guo, L.J. Wan, Angew. Chem. Int. Ed. 52 (2013) 13186–13200.
[9] J. Zheng, J. Tian, D. Wu, M. Gu, W. Xu, C. Wang, F. Gao, M.H. Engelhard, J.-G. Zhang, J. Liu, Nano Lett. 14 (2014) 2345–2352.
[10] H.J. Peng, Q. Zhang, Angew. Chem. Int. Ed. 54 (2015) 11018–11020.
[11] L. Ji, M. Rao, H. Zheng, L. Zhang, Y. Li, W. Duan, J. Guo, E.J. Cairns, Y. Zhang, J. Am. Chem. Soc. 133 (2011) 18522–18525.
[12] Z. Wang, Y. Dong, H. Li, Z. Zhao, H.B. Wu, C. Hao, S. Liu, J. Qiu, X.W.D. Lou, Nat. Commun. 5 (2014) 5002.
[13] Q. Pang, D. Kundu, M. Cuisinier, L. Nazar, Nat. Commun. 5 (2014) 4759.
[14] X. Tao, J. Wang, Z. Ying, Q. Cai, G. Zheng, Y. Gan, H. Huang, Y. Xia, C. Liang, W. Zhang, Nano Lett. 14 (2014) 5288–5294.
[15] Cl Barchasz, F. Molton, C. Duboc, J.-C. Leprêtre, Sb Patoux, F. Alloin, Anal. Chem. 84 (2012) 3973–3980.
[16] J. Song, M.L. Gordin, T. Xu, S. Chen, Z. Yu, H. Sohn, J. Lu, Y. Ren, Y. Duan, D. Wang, Angew. Chem. 127 (2015) 4399–4403.
[17] X. Liang, A. Garsuch, L.F. Nazar, Angew. Chem. Int. Ed. 54 (2015) 3907–3911.
[18] Q. Fan, W. Liu, Z. Weng, Y. Sun, H. Wang, J. Am. Chem. Soc. 137 (2015) 12946–12953.
[19] W. Guo, Y. Yin, S. Xin, Y. Guo, L. Wan, Energy Environ. Sci. 5 (2012) 5221–5225.
[20] H.A. López-Peña, L.S. Hernández-Muñoz, J. Cardoso, F.J. González, I. González, C. Frontana, Electrochem. Commun. 11 (2009) 1369–1372.
[21] Y. Li, T. Liu, H. Liu, M.-Z. Tian, Y. Li, Acc. Chem. Res. 47 (2014) 1186–1198.
[22] M.-K. Hung, Y.-H. Wang, C.-H. Lin, H.-C. Lin, J.-T. Lee, J. Mater. Chem. 22 (2012) 1570–1577.
[23] L. Suo, Y.-S. Hu, H. Li, M. Armand, L. Chen, Nat. Commun. 4 (2013) 1481.
[24] Y. Yang, G. Zheng, Y. Cui, Energy Environ. Sci. 6 (2013) 1552–1558.
[25] S.S. Zhang, J. Electrochem. Soc. 159 (2012) A1226–A1229.
[26] Z.W. Seh, Q. Zhang, W. Li, G. Zheng, H. Yao, Y. Cui, Chem. Sci. 4 (2013) 3673–3677.
[27] H. Chen, C. Wang, Y. Dai, S. Qiu, J. Yang, W. Lu, L. Chen, Nano Lett. 15 (2015) 5443–5448.
[28] F. Zeng, W. Wang, A. Wang, K. Yuan, Z. Jin, Y.-s. Yang, ACS Appl. Mater. Inter. (2015), http://dx.doi.org/10.1021/acsami.5b08537.
[29] L. Brus, J. Chem. Phys. 79 (1983) 5566–5571.
[30] C.-G. Zhan, J.A. Nichols, D.A. Dixon, J. Phys. Chem. A 107 (2003) 4184–4195.
[31] H. Chen, C. Wang, W. Dong, W. Lu, Z. Du, L. Chen, Nano Lett. 15 (2014) 798–802.
[32] D.J. Lee, M. Agostini, J.W. Park, Y.K. Sun, J. Hassoun, B. Scrosati, ChemSusChem 6 (2013) 2245–2248.
[33] L. Wang, T. Zhang, S. Yang, F. Cheng, J. Liang, J. Chen, J. Energy Chem. 22 (2013) 72–77.

[34] D. Zheng, X. Zhang, C. Li, M.E. McKinnon, R.G. Sadok, D. Qu, X. Yu, H.-S. Lee, X.-Q. Yang, D. Qu, J. Electrochem. Soc. 162 (2015) A203–A206.

Hongwei Chen is a research assistant professor under supervision of Prof. Liwei Chen at Suzhou Institute of Nanotech and Nanobionics (SINANO), CAS. He received his PhD degree in physical chemistry from SINANO, CAS in 2013. His research interests generally lie in the area of grid-scale energy storage, especially in battery-related technologies.

Changhong Wang is currently a PhD candidate in Mechanical and Materials Engineering at the University of Western Ontario, Canada. He got his B.S. in applied chemistry in 2011 and obtained his M.S. degree in materials engineering in 2014 from University of Science and Technology of China. After graduation he served as a research assistant in Singapore University of Technology and Design. His research interests are high-energy-density lithium sulfur batteries, lithium ion batteries, atomic layer deposition and molecular layer deposition for clean energy, and memristors for neuromorphic computing.

Yafei Dai is an associate professor of computational physics of Nanjing Normal University. She received her PhD degree from George Mason University in 2009. Her research focuses on theoretical study of two dimensional nano-materials and conducting polymers.

Dr. Jun Ge is a R&D manager in Suzhou Sinlion Battery Tech Co., Ltd, and cooperating with Suzhou Institute of Nano-Tech and Nano-Bionics (SINANO), CAS to develop Lithium-sulfur batteries. Dr. Jun Ge had been doing postdoctoral research on electrochemical energy storage in SINANO. He obtained his pH.D. in Technical Institute of Physics and Chemistry, CAS.

Wei Lu is a professor at SINANO, CAS. He received his B. S. and PhD from USTC in 2000 and 2005 respectively. He then worked as a postdoctoral research fellow at Ohio University until 2008. He joined SINANO in 2008. His main research interests involve design, preparation and manufacture of electrochemical energy storage materials and devices.

Jinlong Yang is currently a Changjiang Professor of Chemistry and executive dean of the School of Chemistry and Material Sciences at USTC. He received his PhD degree in condensed matter physics from USTC in 1991. He is the recipient of the Young Chemist award from the Chinese Chemical Society and the national second prize for natural science, and is the supervisor of two PhD students who were the recipients of the award for national excellent doctoral thesis. His research interests focus on the development of first principles methods and their applications to clusters, nanostructures, solid materials, surfaces, and interfaces.

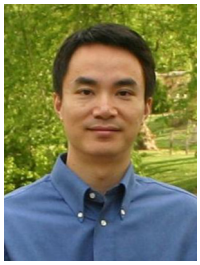

Liwei Chen got his B.S., M.S., and PhD, from University of Science and Technology of China, Peking University, and Harvard University, respectively. After a "bridging" postdoc between Columbia University and IBM T. J. Watson Research Center, he started independent research as an assistant professor at Ohio University in 2004. He moved to Suzhou Institute of Nano-tech and Nano-bionics (SINANO), Chinese Academy of Sciences in 2009. He is currently a Professor of Physical Chemistry, and his research focuses on energy nanotechnology. As an expert in scanning probe microscopy, his approach integrates surface and interface analysis with materials development towards practical applications.